Supporting information

High energy density in combination with high cycling stability in hybrid supercapacitors

Guang Cong Zhang,[a†] Man Feng,[a†] Qing Li,[b] Zhuang Wang,[a] Zixun Fang,[a] Zhimin Niu,[a]

Nianrui Qu,[a] Xiaoyong Fan,[c] Siheng Li,[d] Jianmin Gu,[a]* Jidong Wang[a]* and Desong Wang[a]*

[a]State Key Laboratory of Metastable Materials Science and Technology (MMST), Hebei Key

Laboratory of Applied Chemistry, Hebei Key Laboratory of Heavy Metal Deep-Remediation

in Water and Resource Reuse, Yanshan University, Qinhuangdao, P. R. China

[b]College of Chemistry and Pharmaceutical Engineering, Hebei University of Science and

Technology, Shijiazhuang, 050018, China

[c]School of Materials Science and Engineering, Chang'an University, Xi'an, 710061, China

[d]Shenzhen Jini New Energy Technology Co., Ltd. 3A19, Duchuang Cloud valley, Luozu

Community, Shiyan, Baoan District, Shenzhen, Guangdong, China

†Guang Cong Zhang and Man Feng contributed equally to this work.

E-mail: jmgu@ysu.edu.cn; wangjidong@ysu.edu.cn; dswang06@126.cm

Contents

Figure S1. (a-f) The N_2 absorption-desorption isotherm of the prepared LN samples (0.5 LN-15 LN). The insert is its BJH pore-size distribution curve.
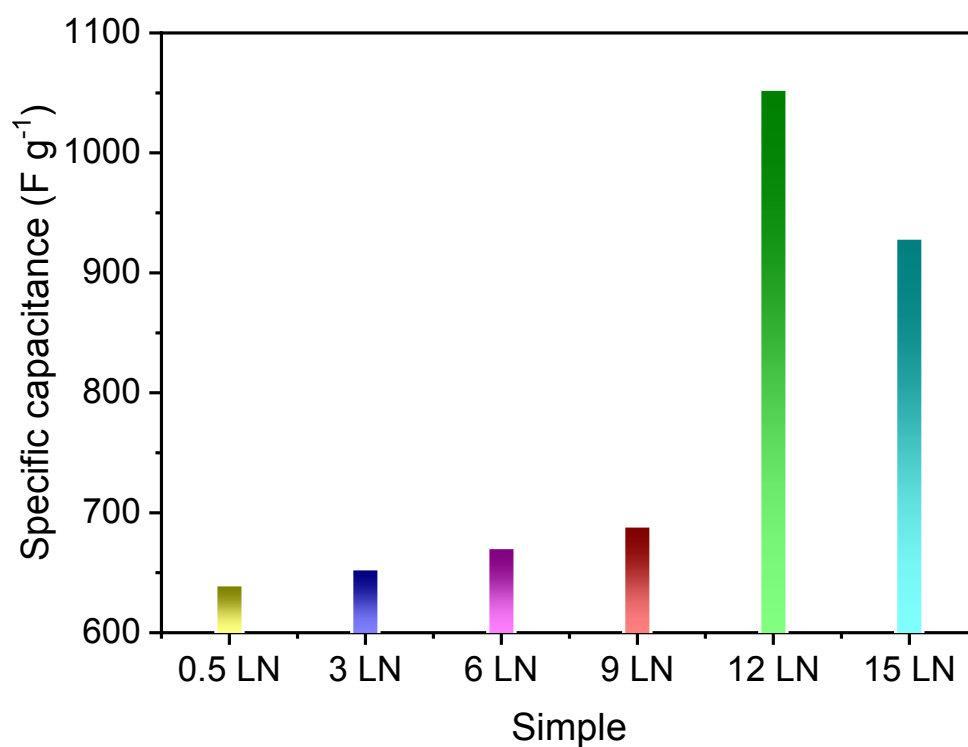
Figure S2. The capacitances of nickel phosphate lamination structure with different number of nanosheets at 0.2 A g^{-1} current densities.

As the Figure S2 shows, the nickel phosphate lamination assembled with 12 h (12 LN) has the largest specific capacitance. This may be due to the higher number of nickel phosphate nanosheets resulting in more activate material to take part in the redox reaction.
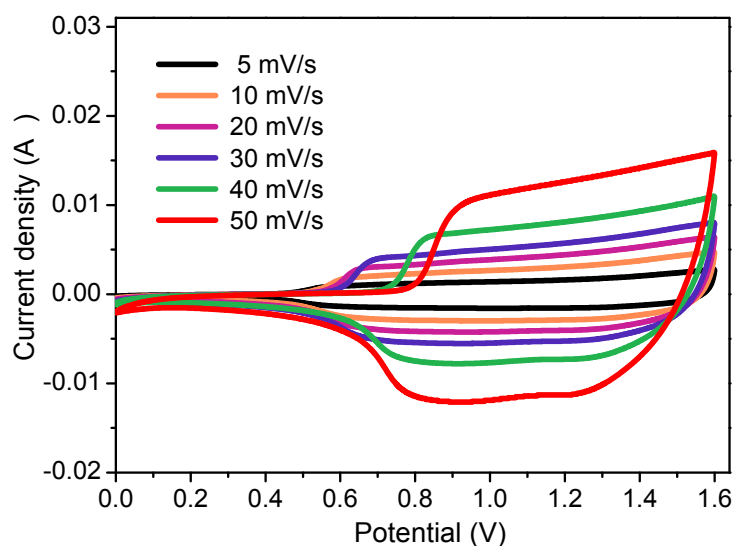
Figure S3. The CV curves of $Ni_3(PO_4)_2 \cdot 8H_2O//C$ (0.5 LN) at scan rates of 5, 10, 20, 30, 40 and 50 mV s^{-1}.

Figure S3 shows the CV curves of $Ni_3(PO_4)_2 \cdot 8H_2O//C$ (0.5 LN) full device at differentscan rates within a cell voltage window of 0-1.6 V. The quasirectangular shapes of these CV curves demonstrate the dominant capacitive behavior rather than battery characteristics. The CV curves retain the same shape with increasing scan rate, which exhibited a good rate capability of the hybrid supercapattery.

Figure S4. The CV curves of $Ni_3(PO_4)_2 \cdot 8H_2O//C$ (3 LN) at scan rates of 5, 10, 20, 30, 40 and 50 mV s^{-1}.

Figure S4 shows the CV curves of $Ni_3(PO_4)_2 \cdot 8H_2O//C$ (3 LN) full device at differentscan rates within a cell voltage window of 0-1.6 V. The quasirectangular shapes of these CV curves demonstrate the dominant capacitive behavior rather than battery characteristics. The CV curves retain the same shape with increasing scan rate, which exhibited a good rate capability of the hybrid supercapattery.

Figure S5. The CV curves of $Ni_3(PO_4)_2 \cdot 8H_2O//C$ (6 LN) at scan rates of 5, 10, 20, 30, 40 and 50 mV s^{-1}.

Figure S5 shows the CV curves of $Ni_3(PO_4)_2 \cdot 8H_2O//C$ (6 LN) full device at differentscan rates within a cell voltage window of 0-1.6 V. The quasirectangular shapes of these CV curves demonstrate the dominant capacitive behavior rather than battery characteristics. The CV curves retain the same shape with increasing scan rate, which exhibited a good rate capability of the hybrid supercapattery.
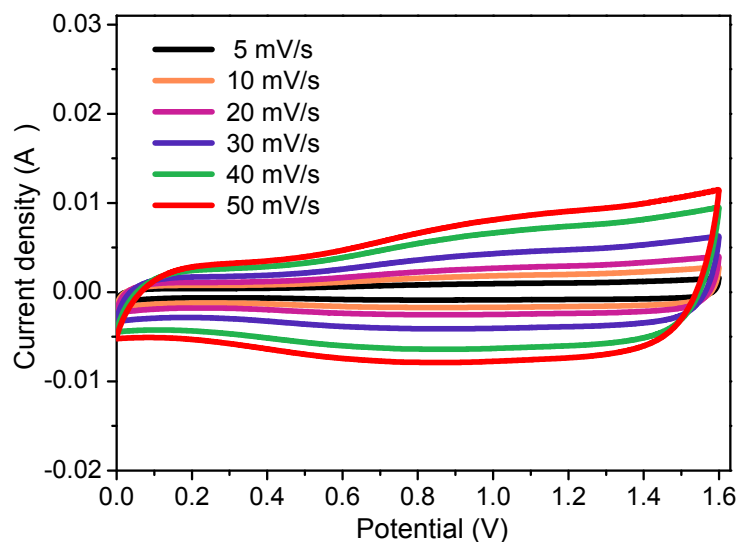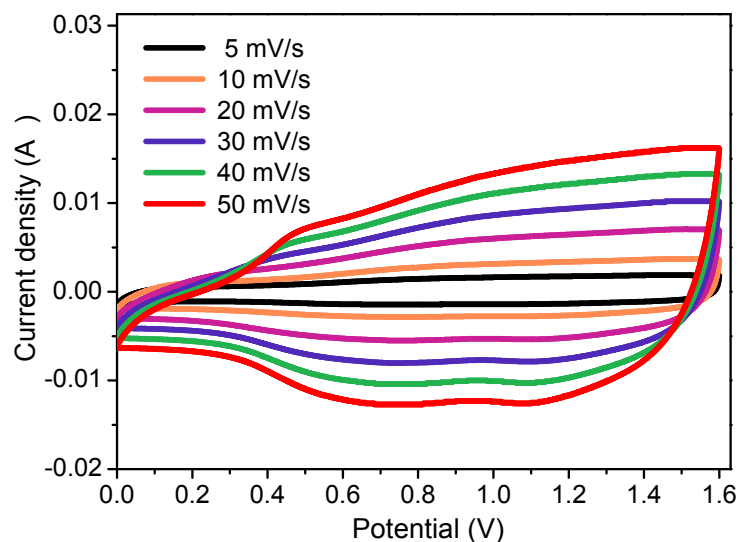
Figure S6. The CV curves of $Ni_3(PO_4)_2 \cdot 8H_2O//C$ (9 LN) at scan rates of 5, 10, 20, 30, 40 and 50 mV s^{-1}.

   Figure S6 shows the CV curves of $Ni_3(PO_4)_2 \cdot 8H_2O//C$ (9 LN) full device at differentscan rates within a cell voltage window of 0-1.6 V. The quasirectangular shapes of these CV curves demonstrate the dominant capacitive behavior rather than battery characteristics. The CV curves retain the same shape with increasing scan rate, which exhibited a good rate capability of the hybrid supercapattery.
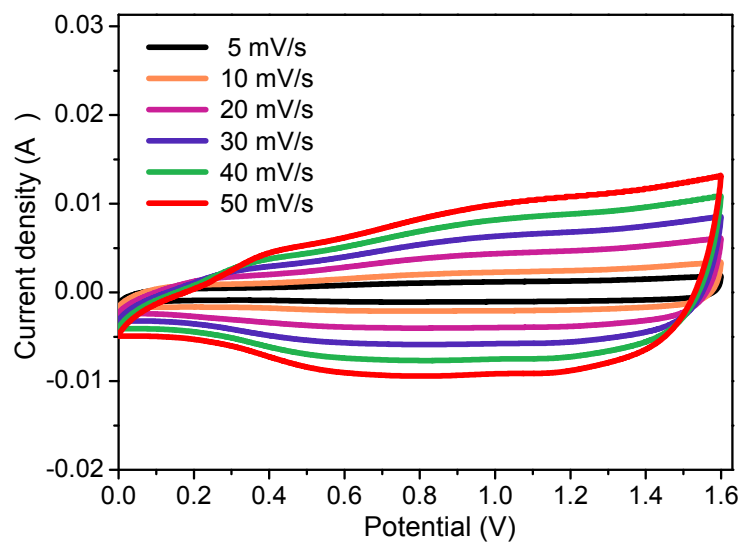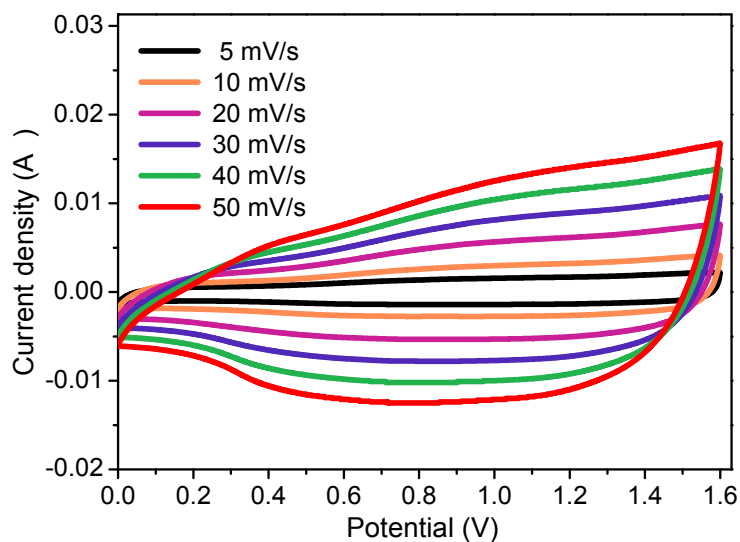
Figure S7. The CV curves of $Ni_3(PO_4)_2 \cdot 8H_2O//C$ (15 LN) at scan rates of 5, 10, 20, 30, 40 and 50 mV s^{-1}.

Figure S7 shows the CV curves of $Ni_3(PO_4)_2 \cdot 8H_2O//C$ (15 LN) full device at differentscan rates within a cell voltage window of 0-1.6 V. The quasirectangular shapes of these CV curves demonstrate the dominant capacitive behavior rather than battery characteristics. The CV curves retain the same shape with increasing scan rate, which exhibited a good rate capability of the hybrid supercapattery.
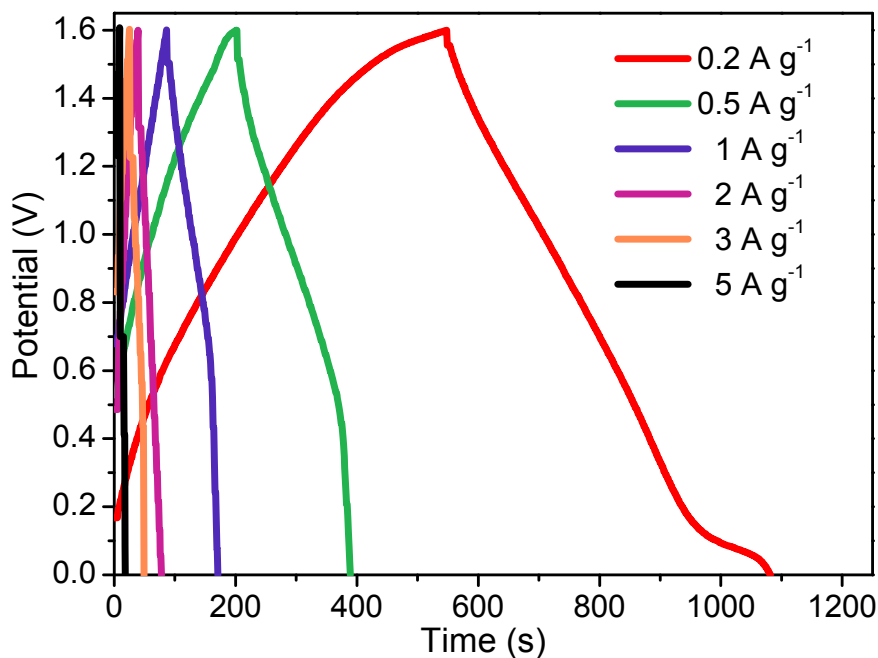
Figure S8. The galvanostatic charge-discharge curves of $Ni_3(PO_4)_2·8H_2O//C$ (0.5 LN) at the current densities of 0.2, 0.5, 1, 2, 3 and 5 A g^{-1}.

Figure S8 shows the charge-discharge curves of the $Ni_3(PO_4)_2·8H_2O//C$ (0.5 LN) supercapattery at different current densities with a cell voltage up to 1.6 V. Quasi-lined charge and discharge curves rather than potential plateaus confirm the capacitive characteristic of the hybrid supercapattery.

Figure S9. The galvanostatic charge-discharge curves of $Ni_3 (PO_4)_2 \cdot 8H_2O//C$ (3 LN) at the current densities of 0.2, 0.5, 1, 2, 3 and 5 A g^{-1}.

Figure S9 shows the charge-discharge curves of the $Ni_3 (PO_4)_2 \cdot 8H_2O//C$ (3 LN) supercapattery at different current densities with a cell voltage up to 1.6 V. Quasi-lined charge and discharge curves rather than potential plateaus confirm the capacitive characteristic of the hybrid supercapattery.

Figure S10. The galvanostatic charge-discharge curves of $Ni_3(PO_4)_2 \cdot 8H_2O//C$ (6 LN) at the current densities of 0.2, 0.5, 1, 2, 3 and 5 A g^{-1}.

Figure S10 shows the charge-discharge curves of the $Ni_3(PO_4)_2 \cdot 8H_2O//C$ (6 LN) supercapattery at different current densities with a cell voltage up to 1.6 V. Quasi-lined charge and discharge curves rather than potential plateaus confirm the capacitive characteristic of the hybrid supercapattery.
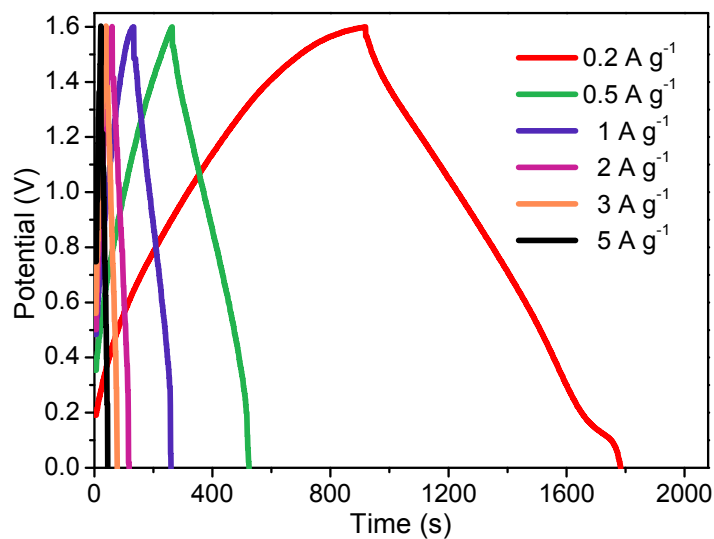
Figure S11. The galvanostatic charge-discharge curves of $Ni_3 (PO_4)_2 \cdot 8H_2O//C$ (9 LN) at the current densities of 0.2, 0.5, 1, 2, 3 and 5 A g^{-1}.

Figure S11 shows the charge-discharge curves of the $Ni_3 (PO_4)_2 \cdot 8H_2O/C$ (9 LN) supercapattery at different current densities with a cell voltage up to 1.6 V. Quasi-lined charge and discharge curves rather than potential plateaus confirm the capacitive characteristic of the hybrid supercapattery.
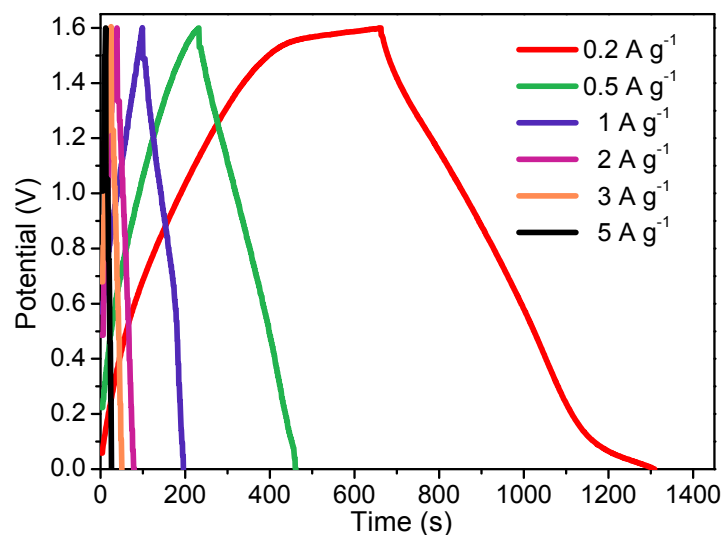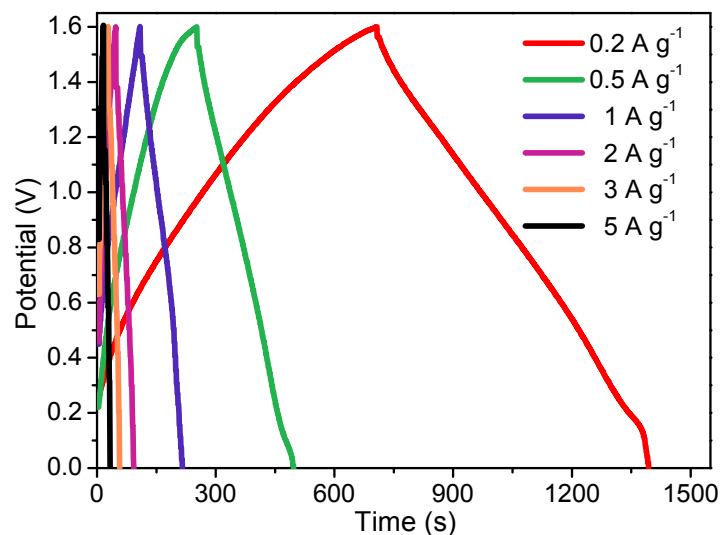
Figure S12. The galvanostatic charge-discharge curves of $Ni_3 (PO_4)_2 \cdot 8H_2O//C$ (15 LN) at the current densities of 0.2, 0.5, 1, 2, 3 and 5 A g^{-1}.

Figure S12 shows the charge-discharge curves of the $Ni_3 (PO_4)_2 \cdot 8H_2O//C$ (15 LN) supercapattery at different current densities with a cell voltage up to 1.6 V. Quasi-lined charge and discharge curves rather than potential plateaus confirm the capacitive characteristic of the hybrid supercapattery.
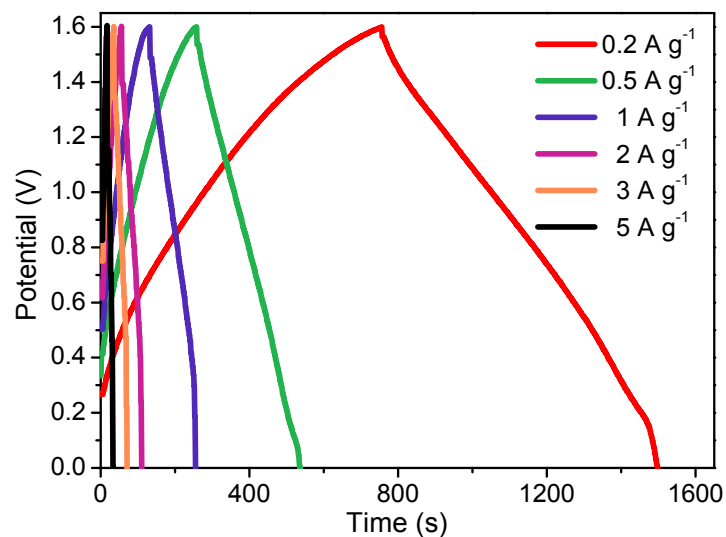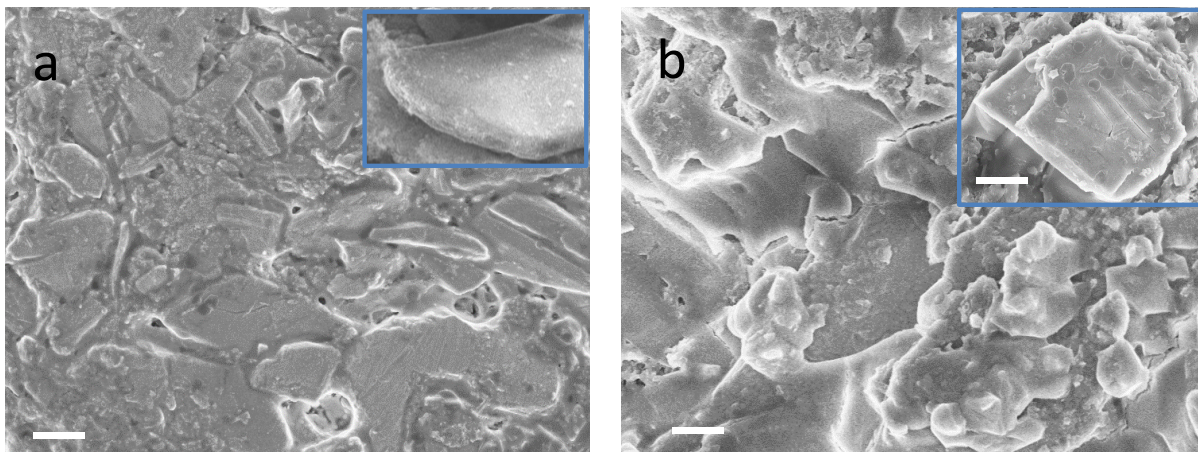
Figure S13. (a-b) SEM images of the nickel phosphate before and after charging/discharging for 8000 cycles. Scale bars are 20 μm for (a) and 10 μm for (b).

The capacity decreased gradually when the charge discharge cycling test continued, which may result from the changes in the structures of the active electrode materials during the long cycling period. The expansion and shrinkage of the composite electrode upon insertion/desertion of anion ion (OH$^-$) of electrolyte into the nickel phosphate lamination, leading to the decomposition and/or loss of the active materials and the crack between the electrode and the current collect, would have a great influence on the cycling life and stability.

Table S1. Cycling stability of half cells with 12 LN $Ni_3(PO_4)_2 \cdot 8H_2O$ and recently reported values for comparison.

Electrode materials	Current density (A g)	Capacitance (F g^{-1})	Capacity (C g^{-1})	Retention	Reference
$Ni_3(PO_4)_2 \bullet 8H_2O$	2	1053	473.9	93% after 2000 cycles 89% after 5000 cycles	This work
$Co_{11}(HPO_3)_8(OH)_6$	1.25	312	Not mention	89.4% after 3000 cycles	24
$Mn_3(PO_4)_2$	0.5	194	Not mention	88.9% after 10000 cycles	25
$NH_4CoPO_4 \cdot H_2O$	0.625	369.4	Not mention	99.7% after 400 cycles	26
$Ni_3(PO_4)_2 \cdot 8H_2O$	2	1301	Not mention	83.59% after 1000 cycles	27
$CoHPO_4 \cdot 3H_2O$	1.5	413	Not mention	85.1% after 3000 cycles	28
Hybrid material of $(Ni,Co)_3(PO_4)_2 \cdot 8H_2O$ and $(NH_4)(Ni,Co)PO_4 \cdot 0.67H_2O$	0.5	1128	Not mention	Not mention	29
MOF-$Ni_xP_yO_2$	1	1627	Not mention	76.82% after 1000 cycles	30
$Co_3(PO_4)_2 \cdot 8H_2O$	1	350	Not mention	1A/g 102% after 1000 cycles	31
$NiCo_2(PO_4)_2$	2	918.14	Not mention	84.5% after 1000 cycles	32
$Ni_3P_2O_8$	0.5	1464	Not mention	84% after 1000 cycles	33

Table S2 Cycling stability of $Ni_3(PO_4)_2 \cdot 8H_2O$//AC and recently reported values for comparison

Positive electrode materials	Negative electrode materials	Current density (A g)	Capacitance (F g^{-1})	Retention	Reference
$Ni_3(PO_4)_2 \cdot 8H_2O$	Activated carbon	0.2	118	94% after 8000 cycles	This work
$Ni_3(PO_4)_2$/RGO/$Co_3(PO_4)_2$	Activated carbon	0.12	115.4	91.9% after 18000 cycles	36
$Co_3(PO_4)_2 \cdot 8H_2O$	Activated carbon	5 mA cm^{-2}	111.2	77.9% after 1000 cycles	40
Nickel-cobalt phosphate composite	Activated carbon	1	162.8	80.4% after 5000 cycles	41
$Co_{0.2}Ni_{0.8}$ pyrophosphate	Activated carbon	1	119	80% after 2000 cycles	42
$Ni_2P_2O_7$	highly porous graphitic carbon	1	183	83% after 2000 cycles	43
$Ni_3P_2O_8$	$Fe_3P_2O_8 \cdot 8H_2O$	0.5	94	81% after 10000 cycles	33
$Mn_3(PO_4)_2$	Activated carbon	0.5	41.9	92% after 8000 cycles	25
NH_4CoNiP	hierarchical porous carbon	0.2	76	95.6% after 5000 cycles	29
$KCo_{0.33}Ni_{0.67}PO_4 \cdot H_2O$	Activated carbon	1.5	227	96% after 5000 cycles	44
$Mn_3(PO_4)_2$	Activated carbon	0.5	28	96% after 10000 cycles	45